

Pressure induced separation of phase-transition-triggered-abrupt vs gradual components of spin crossover

Reece G. Miller,^a Suresh Narayanswamy,^b Simon M. Clark,^c Przemslaw Dera,^d Geoffrey B. Jameson,^e Jeffery L. Tallon^b and Sally Brooker*^a

^a Department of Chemistry and MacDiarmid Institute for Advanced Materials and Nanotechnology, University of Otago, P.O. Box 56, Dunedin 9054, New Zealand

^b MacDiarmid Institute for Advanced Materials and Nanotechnology and Robinson Research Institute, Victoria University of Wellington, P.O. Box 33436, Lower Hutt, New Zealand

^c Department of Earth and Planetary Sciences, Macquarie University, North Ryde, NSW 2109, Australia and The Bragg Institute, Australian Nuclear Science and Technology Organization, Locked Bag 2001, Kirrawee DC, NSW 2232, Australia

^d Hawaii Institute of Geophysics and Planetology, 1680 East West Road, Honolulu, Hawaii 96822, USA

^e Chemistry – Institute of Fundamental Sciences, Massey University, Private Bag 11 222, Palmerston North 4442, New Zealand.

Electronic Supporting Information

Table S1. Crystal system, space group, and cell constants for [Co^{II}(dpzca)₂] at ambient pressure (298 and 90 K; 10⁵ Pa ≡ 0.1 MPa ≡ 1x10⁻⁴ GPa)¹ and at ambient temperature (293 K, 0.42(2) GPa and 1.78(9) GPa).

	10 ⁵ Pa HS (298 K) ^{ab}	10 ⁵ Pa LS (90 K)	0.42 GPa (293 K)	1.78 GPa (293 K)
Crystal system	Tetragonal	Monoclinic	Monoclinic	Monoclinic
Space group	<i>I</i> 14 ₁ / <i>a</i> 1 ^a	<i>P</i> 2 ₁ / <i>c</i>	<i>P</i> 2 ₁ / <i>c</i>	<i>P</i> 2 ₁ / <i>c</i>
<i>a</i> axis (Å)	8.795(2)	8.668(5)	8.610(5)	8.556(5)
<i>b</i> axis (Å) ^a	27.918(9)	27.656(14)	27.630(14)	26.630(14)
<i>c</i> axis (Å) ^a	8.795(2)	8.514(5)	8.444(5)	8.130(5)
<i>β</i> angle (°)	90	91.52(3)	91.66(3)	90.80(3)
Volume (Å ³)	2160(1)	2040(2)	2008(2)	1852(2)

[a]Note that the *b* and *c* axes in the tetragonal HS (298 K and 10⁵ Pa) structure have been swapped to facilitate comparison with the monoclinic structures. [b]Cell parameters (293 K) for the crystal brought back from high pressure to ambient: *a* = *c* = 8.792(1), *b* = 27.916(9), *α* = *β* = *γ* = 90° and *V* = 2158 (1) Å³.

Supplementary Crystallographic Details

Table S2. Selected structural data for $[\text{Co}^{\text{II}}(\text{dpzca})_2]$ under hydrostatic pressure of 0.42(2) GPa, 1.78(9) GPa and 10^5 Pa (after the two high pressure datasets)

	$[\text{Co}^{\text{II}}(\text{dpzca})_2]$		
	0.42(2) GPa	1.78(9) GPa	10^5 Pa (after)
Wavelength [nm]	0.4133	0.4133	0.4133
Empirical formula	$\text{C}_{20}\text{H}_{12}\text{N}_{10}\text{CoO}_4$	$\text{C}_{20}\text{H}_{12}\text{N}_{10}\text{CoO}_4$	$\text{C}_{20}\text{H}_{12}\text{N}_{10}\text{CoO}_4$
M_r	515.33	515.33	515.33
Crystal system	monoclinic	monoclinic	tetragonal
Space group	$P2_1/c$	$P2_1/c$	$I4_1/a$
a [Å]	8.610(5)	8.556(5)	8.792(1)
b [Å]	27.630(14)	26.630(14)	8.792(1)
c [Å]	8.444(5)	8.130(5)	27.916(9)
α [°]	90	90	90
β [°]	91.66(3)	90.80(3)	90
γ [°]	90	90	90
V [Å ³]	2008(2)	1852.2(18)	2157.9(12)
Z	4	4	16
T [K]	293(2)	293(2)	293(2)
$\rho_{\text{calcd.}}$ [gcm ⁻³]	1.678	1.848	1.586
μ [mm ⁻¹]	0.474	0.552	0.45
Completeness to θ [%]	14.9	18.2	34.4
Redundancy	1.6	3.0	3.5
$R\sigma$	0.0924	0.0772	0.1794
$F(000)$	1044	1044	1044
θ range [°]	1.82 to 14.14	1.59 to 12.13	1.79 to 14.29
Reflections collected	933	822	1206
Independent reflections	580	273	340
$R(\text{int})$	0.0629	0.1211	0.3096
Data/ restraints/ parameters	580 / 0 / 146	273 / 149 / 141	340 / 0 / 80
Goof (F^2)	1.060	1.376	1.140
R_I [$I > 2\sigma(I)$]	0.0576	0.1030	0.0610
wR_2 [$I > 2\sigma(I)$]	0.1212	0.2864	0.1456
R_I [all data]	0.0599	0.1042	0.0607
wR_2 [all data]	0.1219	0.2870	0.1459
Largest diff. peak and hole [eÅ ⁻³]	0.265 and -0.212	0.418 and -0.427	0.287 and -0.318

Supplementary refinement details

[Co^{II}(dpzca)₂] at 0.42(2) GPa and room temperature

At this pressure the entire molecule of [Co^{II}(dpzca)₂] is present in the asymmetric unit. No solvent. No disorder. Due a very low data:parameter ratio all atoms were refined isotropically with the exception of Co(1). All H-atoms are riding in calculated positions. No restraints were required to get a stable refinement.

[Co^{II}(dpzca)₂] at 1.78(9) GPa and room temperature

At this pressure the entire molecule of [Co^{II}(dpzca)₂] is present in the asymmetric unit. No solvent. No disorder. Due a very low data:parameter ratio all atoms were refined isotropically. Additionally restraints were required in order to get a stable refinement. DFIX was used to restrain the C-C (1.40 Å) and C-N (1.35 Å) bond lengths between adjacent atoms in all four pyrazine rings. SADI was used to restrain the distances between non-adjacent atoms in all four pyrazine rings to be approximately equal. FLAT was used to restrain all four pyrazine rings to a plane. Both imide functionalities were also restrained into a plane using FLAT and the C-O (1.22 Å) and C-N (1.37 Å) bonds were restrained using DFIX. Additionally SADI was used to restrain the imide O to imide N distances to be approximately equal on both ligand strands. The Co-N distances on trans donors were also restrained to be approximately equal using SADI. The twin law TWIN -100 0-10 001 was used to allow for twinning (BASF 0.07624). All H-atoms are riding in calculated positions.

Note that an exactly parallel refinement of the 0.42(2) GPa dataset using the restraints employed here gave bond lengths and angles insignificantly different to those which were observed without the restraints. This provides evidence that the large number of restraints required to get a stable refinement at 1.78(9) GPa does not produce any artifacts.

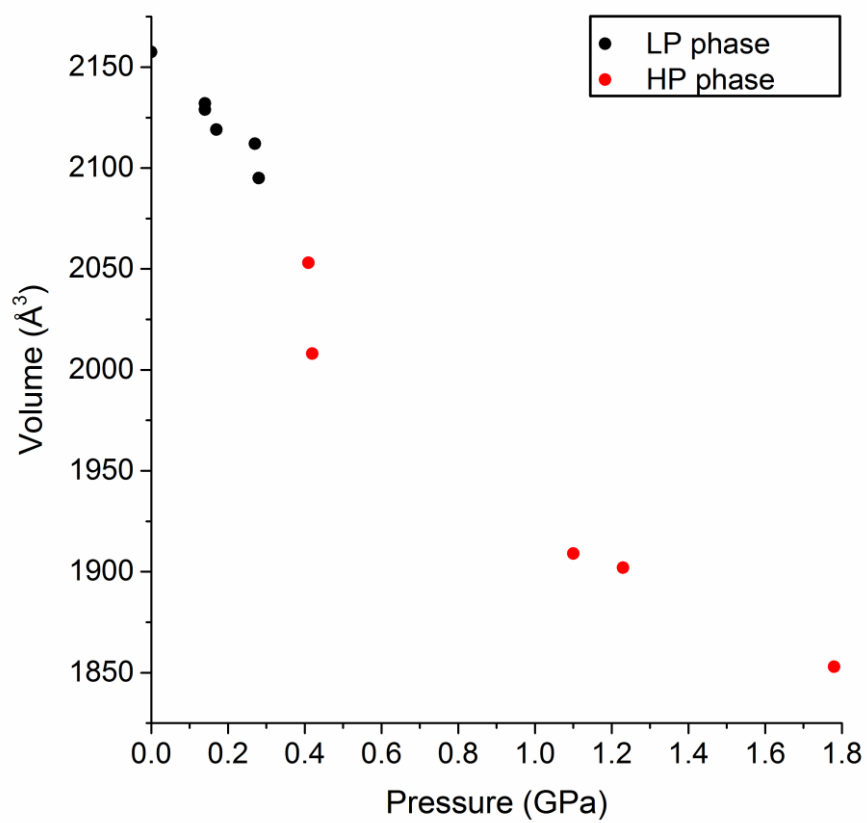


Figure S1. Unit cell volume of [Co^{II}(dpzca)₂] as a function of applied hydrostatic pressure.

Supplementary structural figures

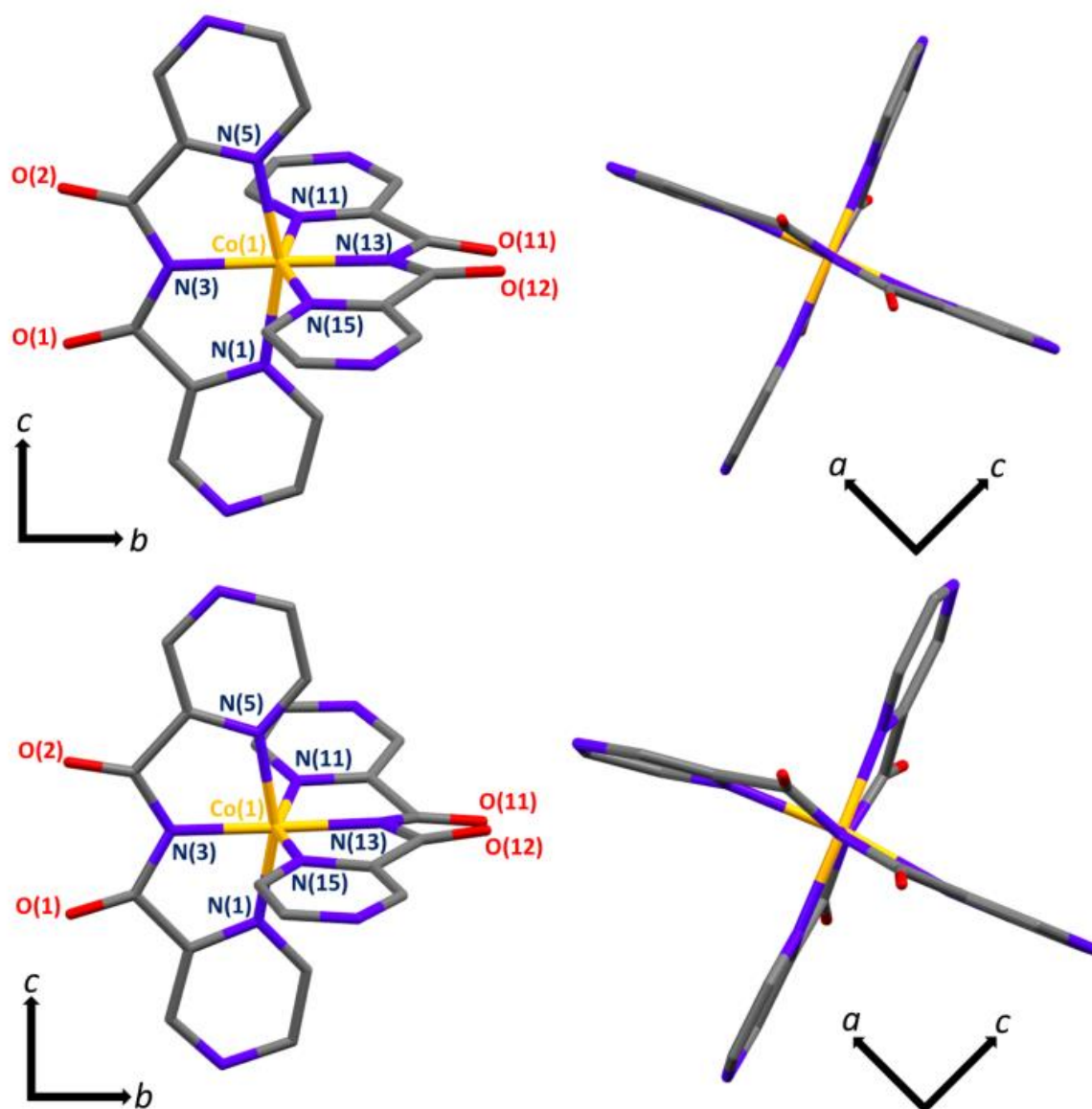


Figure S2. Solid-state structure of $[\text{Co}^{\text{II}}(\text{dpzca})_2]$ at room temperature (293 K) under an applied hydrostatic pressure of (top) 0.42(2) GPa and (bottom) 1.78(9) GPa, as viewed down the *a* axis (left) and *b* axis (right).

Additional discussion of details of structural features under pressure

Monitoring the unit cell constants as the hydrostatic pressure on a single crystal of $[\text{Co}^{\text{II}}(\text{dpzca})_2]$ was increased in 10 steps from ambient to 1.78(9) GPa, at room temperature, clearly revealed a structural phase transition at about 0.4 GPa. An X-ray crystal structure data collection at 0.42(2) GPa (293 K) yielded a structure with cobalt(II) bond lengths and angles consistent with Jahn-Teller distorted, mostly LS cobalt(II), similar to the structure of the thermally induced (90 K, ambient pressure) LS form. On the other hand, at 1.78(9) GPa a fully low-spin structure with significantly increased out-of-plane distortion of the conjugated terdentate ligand was revealed. At 1.78 GPa, the pressure is causing significant distortions to the complex and these are correlated to the substantially different pressure sensitivity of the a and c unit cell lengths, which were equivalent in the HS tetragonal crystal system (again making the tetragonal b axis unique for ease of comparison with the monoclinic low-spin structures).

The short Co-N bonds at 1.78 GPa cause loss of planarity of the conjugated terdentate pyrazine imide ligand strand: the pyrazine rings within each ligand strand are twisted by 6.5° (ligand 1) and 9.7° (ligand 2) relative to one another (Figure S2) compared to 5.4 and 3.6° in the 0.42 GPa structure, and 3.5 and 3.7° in the 90 K structure (Figure S2). Also, the mean plane of one of the pyrazine rings on the, Jahn-Teller elongated, 2nd ligand strand [the N11 ring], has shifted significantly further out of the equatorial plane of donors to which it contributes, making an angle of 16.9° in the 1.8 GPa structure, rather than just 3.3° in the 0.42 GPa and 90 K structures (Figure S3). It is also interesting to note that the octahedral distortion parameter for the unequivocally LS (Table 2) cobalt(II) center at 1.78 GPa, $\Sigma = 99^\circ$, reflects these increased ligand distortions, as it is significantly higher than at 0.42 GPa (90°) or at 90 K (76° , ambient pressure), and is approaching that observed for the HS structure, (111° , ambient temperature and pressure).

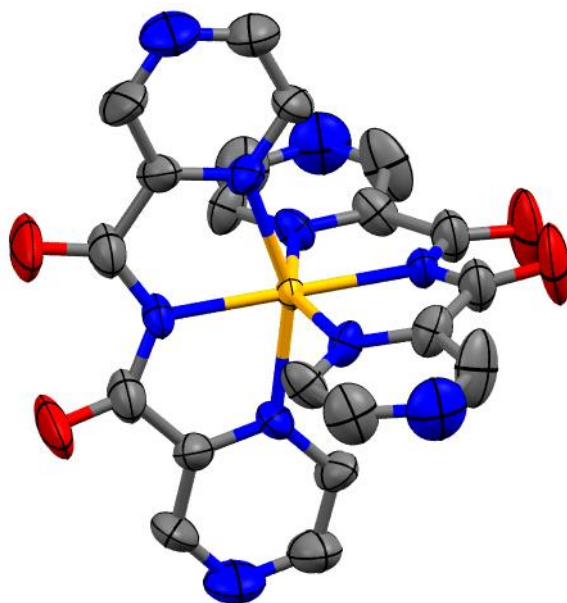


Figure S3. Solid state structure of $[\text{Co}(\text{dpzca})_2]$ at ambient temperature and pressure after the collection of the high pressure datasets. Thermal ellipsoids are shown at the 50% probability level.

Supplementary magnetic details

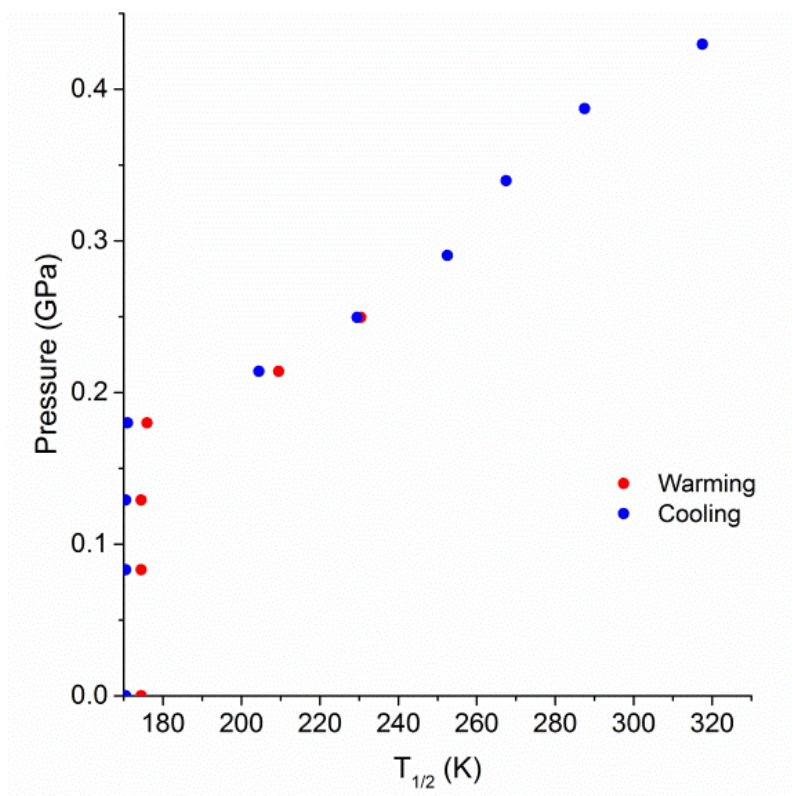


Figure S4. P vs $T_{1/2}$ plot (see paper for the $T_{1/2}$ vs P plot).

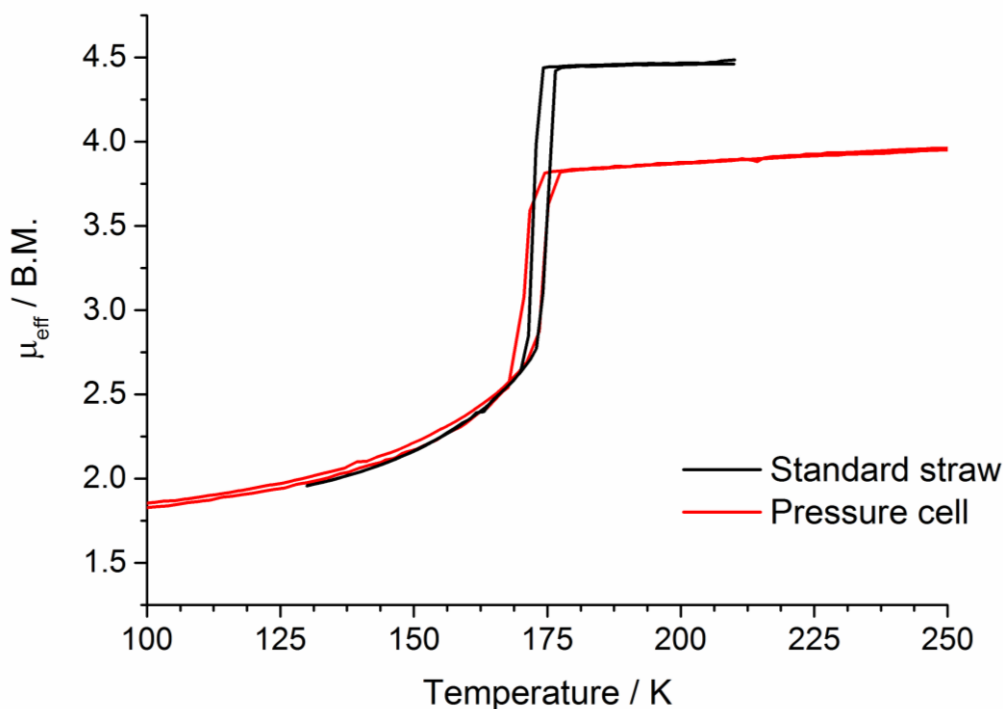


Figure S4. Comparison of the magnetic moment as a function of temperature for $[\text{Co}^{\text{II}}(\text{dpzca})_2]$ as measured in a standard MPMS straw (black) and the homebuilt pressure cell (red). The consistency of the shape of the temperature response suggests that the difference in the absolute value is an artefact of the limitations of correcting for the pressure cell holder.

Additional discussion of details of magnetic response under pressure

The magnetic data show that the single-step abrupt and hysteretic SCO event seen at ambient pressure separates on increasing the pressure, into a combination of an underlying gradual SCO and an abrupt SCO at higher temperature. The abrupt component of the SCO event in $[\text{Co}^{\text{II}}(\text{dpzca})_2]$ can be shifted to ambient temperature with the application of a hydrostatic pressure of more than 0.4 GPa. The magnetic measurements, Raman spectroscopy and crystallographic data are all consistent with the abrupt SCO event being associated with the crystallographic phase transition from $I4_1/a$ to $P2_1/c$. The application of pressure shifts this crystallographic phase transition to higher temperatures, removing the barrier to SCO at low temperatures, and therefore allowing the observation of the, previously unresolved, underlying gradual SCO.

At higher temperatures it is still favorable for the majority of the cobalt(II) centers to be in the HS state and hence the abrupt process makes up a smaller proportion of the overall SCO event.

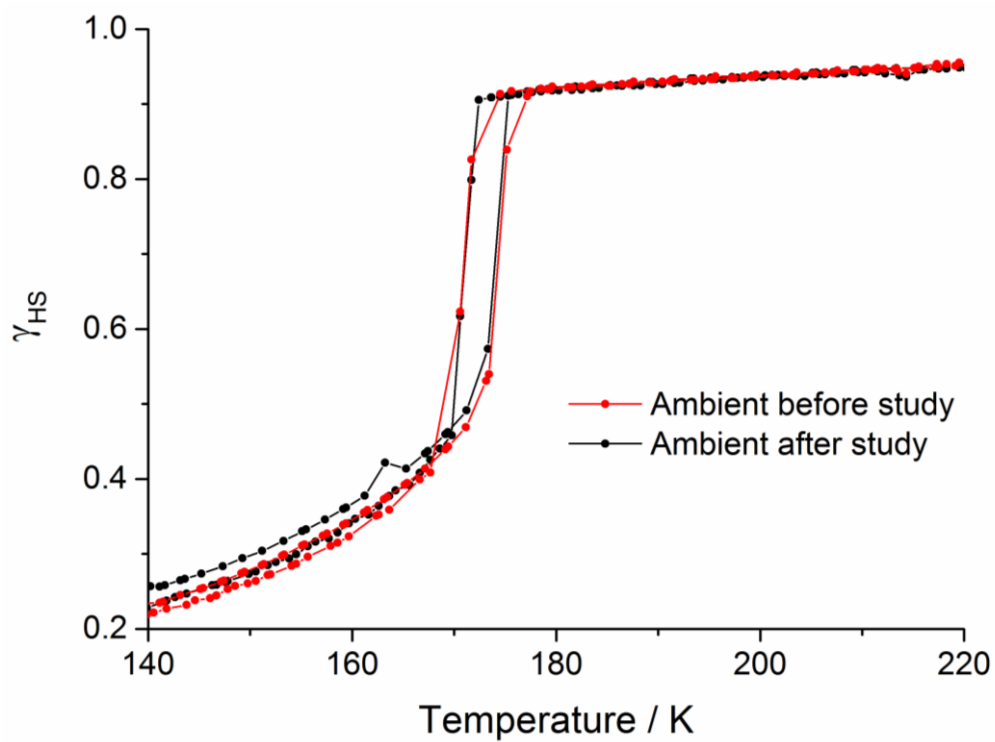


Figure S5. Fraction HS (γ_{HS}) vs temperature for $[\text{Co}^{\text{II}}(\text{dpzca})_2]$ before and after the pressure study confirming reversibility in the response to applied pressure.

Magnetic details of some other spin crossover active cobalt(II) complexes at ambient P

Table S3. Survey of hysteretic spin crossover in cobalt(II) complexes, noting $T_{1/2\downarrow} / T_{1/2\uparrow}$ and the associated crystallographic phase transitions. ^aNot Structurally characterized in both spin states. ^b Assumed – not structurally characterized in both states but is physically impossible not to involve a phase transition. ^c Phase transition not assigned but X-ray powder diffraction shows that it occurs.

	$T_{1/2\downarrow} / T_{1/2\uparrow}$	Type of SCO	Phase Transition LS \rightarrow HS
$\{\text{Co}^{\text{II}}[\text{H}_2(\text{fsa})_2\text{en}](\text{py})_2\}^9$	115/127	Normal	Only HS structure ^a
$\{\text{Co}^{\text{II}}[\text{H}_2(\text{fsa})_2\text{en}](\text{H}_2\text{O})_2\}^{10}$	82/85	Normal	No structures ^a
$\{\text{Co}^{\text{II}}[\text{H}_2(\text{fsa})_2\text{en}](\text{tBupy})_2\}^{11}$	138/154	Normal	No structures ^a
$[\text{Co}^{\text{II}}(\text{C14-terpy})_2](\text{BF}_4)_2 \cdot \text{MeOH}^{12}$	50/50	Normal	No hysteresis
	206/184	Reverse	Long alkyl chain rearrangement
$[\text{Co}^{\text{II}}(\text{OH-C10-terpy})_2](\text{BF}_4)_2$	295/316	Normal	No structures ^a
$[\text{Co}^{\text{II}}(\text{OH-C12-terpy})_2](\text{BF}_4)_2$	308/348	Normal	No structures ^a
$[\text{Co}^{\text{II}}(\text{C5C12C10-terpy})_2](\text{BF}_4)_2$	284/288	Normal	Single crystal \rightarrow Mesophase
$[\text{Co}^{\text{II}}(\text{OH-C14-terpy})_2](\text{BF}_4)_2$	231/214	Reverse	Assumed ^b
$[\text{Co}^{\text{II}}(\text{C14-terpy})_2](\text{BF}_4)_2^{13}$	307/250	Reverse	Yes (PXRD) ^c
$[\text{Co}^{\text{II}}(\text{C16-terpy})_2](\text{BF}_4)_2^{13}$	260/217	Reverse	Yes (PXRD) ^c
$\{[\text{Co}^{\text{II}}(\text{pyterpy})\text{Cl}_2] \cdot \text{H}_2\text{O}\}_n^{14}$	222/223	Normal	No structures ^a
$[\text{Co}^{\text{II}}(\text{4-terpyridone})_2] \cdot (\text{CF}_3\text{SO}_3)_2 \cdot \text{H}_2\text{O}^{15}$	156/189	Normal	Axis doubling ($a \rightarrow 2a$)
	226/215	Reverse	Axis halving ($2a \rightarrow a$)
$[\text{Ar}'\text{Co}^{\text{II}}\text{N}(\text{H})\text{Ar}^{\#}]^{16}$	221/229	Normal	Valence Tautomerism
$[\text{Co}^{\text{II}}(\text{dpzca})_2]^1$	168/178	Normal	$\text{P2}_1/\text{c} \rightarrow \text{I4}_1/\text{a}$

Table S4. The midpoint temperature ($T_{1/2}$) for both the abrupt (\dagger) component of the spin crossover and the overall process at each of the pressures studied (temperatures in K).

Pressure (GPa)	$T_{1/2}\uparrow$ ($\gamma_{HS} = 0.5$)	$T_{1/2}\downarrow$ ($\gamma_{HS} = 0.5$)	$\Delta T_{1/2}$	$\dagger T_{1/2}\uparrow$ Abrupt	$\dagger T_{1/2}\downarrow$ Abrupt	$\Delta \dagger T_{1/2}$
0	173	169	4	174	170	4
0.0832	173	169	4	174	170	4
0.1290	173	169	4	174	170	4
0.1800	173	168	5	176	171	5
0.2139	189	188	1	210	205	5
0.2496	202	202	0	231	230	1
0.2904	214	214	0	253	253	0
0.3396	218	218	0	268	268	0
0.3871	227	227	0	288	288	0
0.4296	235	235	0	318	318	0

Supplementary Raman spectroscopy details

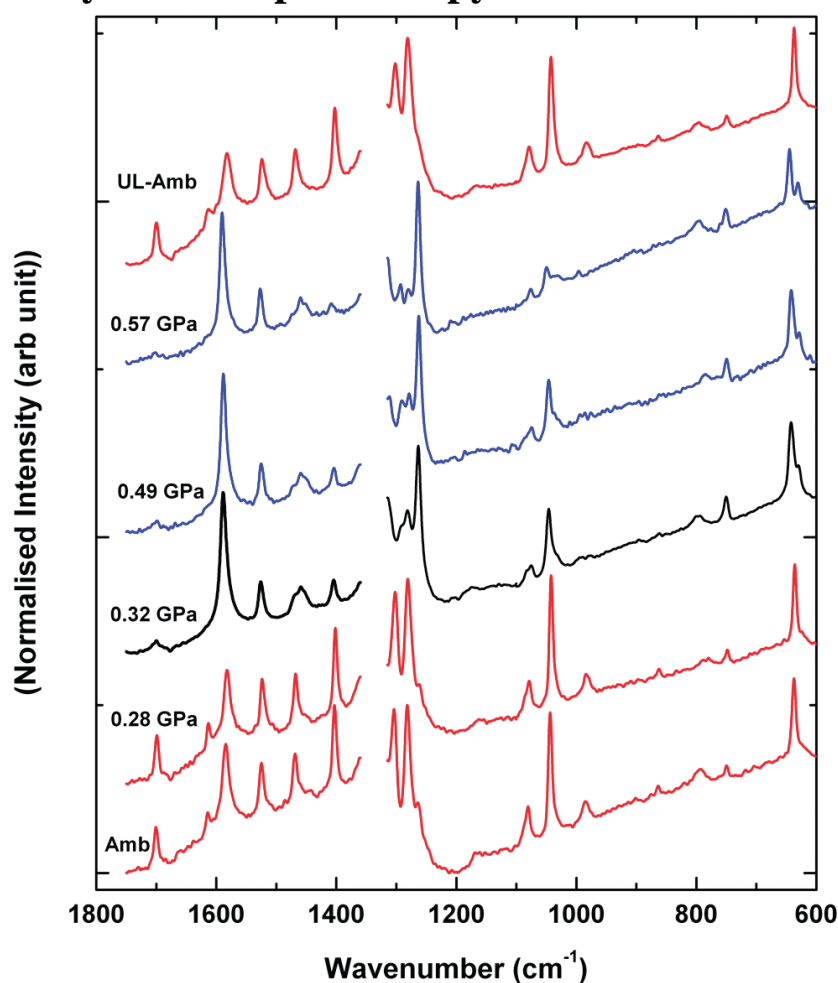


Figure S6. The effect of pressure on the Raman spectrum of $[\text{Co}^{\text{II}}(\text{dpzca})_2]$. Bottom to top: pressure loading spectra at ambient (red line = HS), 0.28 GPa, 0.32 GPa (black line = mixed HS-LS state), 0.49 GPa and 0.57 GPa (blue line = mostly LS state), then ambient after the study. Figure reproduced from reference.¹

Table S5. List of Raman bands observed for [Co^{II}(dpzca)₂] at ambient pressure and 0.3 GPa. Reproduced from reference.¹

Ambient (HS)	0.3 GPa
637.03	628.8
642.7	
750.2	751.2
793.9	791.9
985.3	989.9
1043.9	1045.9
1080.4	1075.8
1264.8	1263.8
1282.5	1276.6
1303.2	1293.8
1310.5	
1402.2	1404.5
1467.3	1458.9
1525.0	1525.9
1582.6	1588.7
1697.9	
1733.6	

References

1. M. G. Cowan, J. Olgúin, S. Narayanaswamy, J. L. Tallon and S. Brooker, *J. Am. Chem. Soc.*, 2012, 134, 2892–2894 and front cover feature.
2. N. Suresh and J. L. Tallon, *Phys. Rev. B*, 2007, 75, 174502.
3. M. Kunz, A. A. MacDowell, W. A. Caldwell, D. Cambie, R. S. Celestre, E. E. Domning, R. M. Duarte, A. E. Gleason, J. M. Glossinger, N. Kelez, D. W. Plate, T. Yu, J. M. Zaug, H. A. Padmore, R. Jeanloz, A. P. Alivisatos and S. M. Clark, *J. Synchrotron Rad.*, 2005, 12, 650-658.
4. R. Boehler and K. De Hantsetters, *High Press. Res.*, 2004, 24, 391-396.
5. H. K. Mao, J. Xu and P. M. Bell, *J. Geophys. Res. [Solid Earth]*, 1986, 91, 4673-4676.
6. R. T. Downs and D. C. Palmer, *Amer. Mineral.*, 1994, 79, 9-14.
7. P. Dera, K. Zhuravlev, V. Prakapenka, M. L. Rivers, G. J. Finkelstein, O. Grubor-Urosevic, O. Tschauner, S. M. Clark and R. T. Downs, *High Press. Res.*, 2013, 33, 466-484.
8. G. M. Sheldrick, *Acta Crystallogr., Section A*, 2008, A64, 112-122.
9. J. Zarembowitch and O. Kahn, *Inorg. Chem.*, 1984, 23, 589-593.
10. J. Zarembowitch, R. Claude and O. Kahn, *Inorg. Chem.*, 1985, 24, 1576-1580.
11. P. Thuery and J. Zarembowitch, *Inorg. Chem.*, 1986, 25, 2001-2008.
12. S. Hayami, K. Murata, D. Urakami, Y. Kojima, M. Akita and K. Inoue, *Chem. Commun.*, 2008, 48, 6510-6512.
13. S. Hayami, Y. Shige-yoshi, M. Akita, K. Inoue, K. Kato, K. Osaka, M. Takata, R. Kawajiri, T. Mitani and Y. Maeda, *Angew. Chem. Int. Ed.*, 2005, 44, 4899-4903.
14. S. Hayami, K. Hashiguchi, G. Juhász, M. Ohba, H. Ōkawa, Y. Maeda, K. Kato, K. Osaka, M. Takata and K. Inoue, *Inorg. Chem.*, 2004, 43, 4124-4126.
15. G. Agustí, C. Bartual, V. Martínez, F. J. Muñoz-Lara, A. B. Gaspar, M. C. Muñoz and J. A. Real, *New J. Chem.*, 2009, 33, 1262-1267.
16. C. Ni, J. C. Fettinger, G. J. Long and P. P. Power, *Inorg. Chem.*, 2009, 48, 2443-2448.